Phase transitions and aging effects of the graphite intercalation compound α-C_{5n}-HNO_3

Emil J. Samuelsen* and Roger Moret
Laboratoire de Physique des Solides, Université de Paris—Sud, F-91405 Orsay, France

Hervé Fuzellier, Martine Klatt, Michèle Lelaurain, and Albert Hérold
Laboratoire de Chimie Minérale Appliquée, Université de Nancy 1, F-54506 Vandoeuvre des Nancy, France
(Received 21 August 1984)

Detailed x-ray studies of nitric acid intercalated in graphite have been carried out, notably on the α-C_{5n}-HNO_3 modification. Single-crystal samples were prepared with staging indices $n=8$, 2, and 3. The material shows a rather complex behavior with pronounced aging effects, which have been identified. The normal, aging-independent phases were found to be the following: Above $\sim$250 K a disordered liquidlike phase exists, which by a first-order transition goes into an ordered phase upon cooling. The transition shows a clear hysteresis ($T_{ch}=249\pm1$ K, $T_{cl}=244\pm1$ K). The ordered phase is incommensurate with the graphite lattice in one unit cell-direction ($\mathbf{A}=1.43\mathbf{a}_G$), but commensurate in the other direction ($\mathbf{B}=2\mathbf{a}_G+9\mathbf{b}_G$). A tendency for a lock-in transition along $\mathbf{A}$ by a supercell 12 times larger was seen from the appearance of super-reflections for the fresh stage-2 and the stage-3 samples, but full commensuration ($\mathbf{A}\simeq17\mathbf{a}_G$) was not achieved. A unique feature of the ordering phase transition in this material is a pronounced sliding motion of the graphite layers out of the normal hexagonal stacking below T_c. The intercalant layers act effectively as ball bearings for this motion. The motion is probably restricted by elastic deformations at the domain walls. Aging effects over a time span of a few months involve a change of staging, the disappearance of an intermediate phase of the low-stage samples, and, maybe most importantly, the growth of an extra ordered phase. The latter phase is commensurate with the graphite lattice and has a separate transition temperature, $T_{cx}=259\pm1$ K. This phase may be the cause of a second peak previously observed in calorimetric studies.

I. INTRODUCTION

Pure nitric acid, HNO_3, readily forms intercalation compounds with graphite (GIC, denoting graphite intercalation compound). The "normal" or α form is known to have a composition close to[1] C_{5n}-HNO_3, where n is the stage index, whereas a "residual" or β form with the composition C_{8n}-HNO_3 is formed from the α form by exposure to air over an extended time.[1] The present work is devoted to studies of the α form.

The scientific interest in α-C_{5n}-HNO_3 is connected to the order-disorder of the intercalant layers taking place at about 250 K. The transition is signaled both in conductivity studies[2,3] and calorimetry,[4] and, in particular, in several x-ray works.[5–9] It should be noted that also the related compound with nitric pentoxide N_2O_5, C_{5n}-N_2O_5, shows very similar behavior.[5]

The calorimetric studies strongly suggested the phase transition to be a discontinuous one, with a hysteresis of several degrees Kelvin. Furthermore, a two-peak calorimetric anomaly, 4—8 K apart, was seen, the detailed behavior being somewhat stage and heat-treatment dependent. Also, the pentoxide compound shows this behavior.[5] The origin of the two peaks has not been understood until now. The early x-ray work by Rüdorff[10] was aimed at understanding the staging and possible molecular orientation within the graphite layers. The proposed double-layer—model ordering of HNO_3 molecules has been questioned,[11] and, in a recent neutron- and resonant γ-ray-scattering experiment by Pinto *et al.*,[12] has been shown to be incorrect. It turns out that the planar HNO_3 molecules enter the intercalant layers with their molecular planes essentially normal to the graphite layers.[11,12] Since the interplanar distance does not change much at the phase transition temperature, an essentially perpendicular orientation is probably preserved at all temperatures.

Details of the staging schemes and the effect of the phase transition were explored in an excellent work by Nixon, Parry, and Ubbelohde.[6] Stacking sequences of graphite layers and their space-group symmetries were determined from x-ray studies of stage-1, -2, -3, and -4 samples, but since only oriented polycrystalline graphite samples were used, not much could be concluded about the low-temperature phase-ordering scheme, except that it is complex. More recent work on single-crystal materials, however, also only concluded that the in-plane ordering is complex.[7,8]

In fact, only very recently have we managed to disentangle the main features of the complex x-ray ($hk0$) pattern of the low-temperature phase, of which a preliminary report has been published.[9]

It is the purpose of this paper to present the α-C_{5n}-HNO_3 GIC as a highly unusual and complicated material, but with some new and unique features. In addition to the large superstructure formation, the complication is partly connected with pronounced sample-aging effects, which must be identified in order to study further the

TABLE I. Sample characteristics.

Sample no.	Size (mm^3)	Method of intercalation	Time elapsed after intercalation	Stage index
1	$0.5\times0.9\times4.5$	Direct contact	13 months	6
		HNO_3 vapor, 25°C	25 months	8
2	$0.5\times1.2\times4$	Direct contact	1 month	2
		HNO_3 vapor, 25°C	5 months	2 (89%); 3 (11%)
3	$0.5\times1.3\times5$	Vapor removal	1 month	2
		before encapsulation	5 months	3 (95.5%); 2 (4.5%)

main structural aspects of the nitric acid intercalant. The aging of our samples involves both staging transitions and changes of commensurability, as well as chemical effects involving an extra "impurity" phase.

A unique feature is the observation that the phase transition at about 250 K involves not only an ordering-disordering of the intercalant, but also a sizable sliding of graphite layers. Diffraction effects related to this unique behavior were in fact already noted by Parry.[7] The sliding motion is abrupt upon passing T_c, and we argue that it may be provoked by molecular tilt motion and is restricted by domain boundary strains. Also, intercalant interlayer correlations have been studied. Details of the in-plane molecular structure will be given in a planned subsequent paper, in which we also discuss the "liquid" structure above T_c.

II. EXPERIMENTAL DETAILS

A. Sample preparation and staging

The samples used were made from single-crystal pieces of natural graphite from Madagascar. The preparation methods and sample characteristics are given in Table I. After preparation, the samples were protected from exposure to the atmosphere by sealing them in thin-walled glass capillary tubes.

The stage index n was determined from x-ray studies of the $00l$ reflections, assuming the "repeat distance" I_c (see Appendix A) along the graphite unique axis to be expressible by[13]

$$I_c(\text{Å})=3.35(n-1)+7.80\ . \tag{1}$$

As indicated in Table I and Appendix A the stage index of sample 3 changed from pure $n=2$ to almost pure $n=3$ during four months. For sample 2, a minority fraction [$(11\pm3)\%$] had transformed from stage 2 to 3. Although this indicates aging effects and long-time instability, it provided an unexpected opportunity to demonstrate essential stage-independence of the main ordering features and the ordering temperatures of α-C_{5n}-HNO_3. Since the samples are encapsuled, no direct compositional check has been performed, but some desorption has most probably taken place, because tiny droplets were found on the walls of the capillary tubes. Checks with x rays showed no evidence of alteration of the sample homogeneity upon aging.

B. Sample quality

Natural single crystals of a soft material such as graphite are usually less perfect than other crystalline materials one is used to dealing with. Furthermore, the cutting and the fitting tightly of the crystal into a narrow capillary tube may distort its edges. With this in mind, the present samples must be characterized as being quite good. In Fig. 1 we reproduce a precession picture containing $00l$ reflections, showing an angular spread of the order of $\pm3°$ in this particular projection. Rocking curves taken with the diffractometer show that the crystallite distribution is dependent on the position on the sample, and they sometimes show the presence of two or three peaks at separations of 1°—2°, each of width about

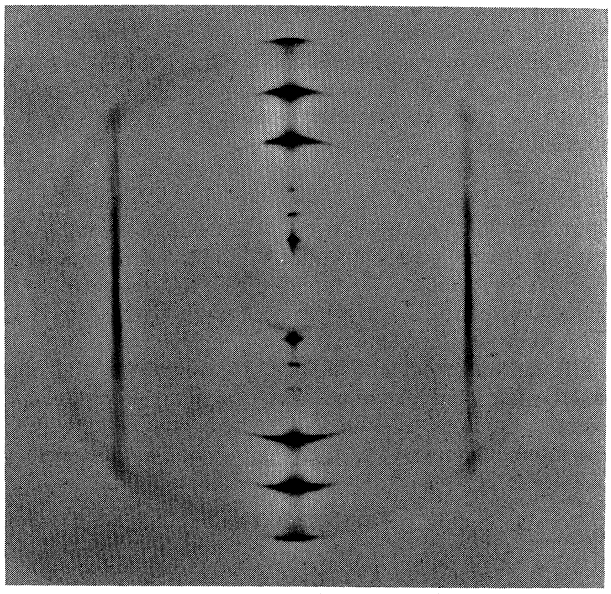

FIG. 1. Precession photograph of fresh sample 2 at 225 K showing a section containing the graphite $(00l)_G$ up to $l=5$, and the intercalant $(10l)_M$, showing l modulation. C-axis mosaic spread is seen.

1°—1.4°. The in-plane mosaic spread is less, that is, 0.4° and 0.5° as measured for the intercalant peaks. Except for truly radial $\omega-2\theta$ scans, the mosaic spread will influence the peak widths of most diffraction scans, and corrections are necessary for proper comparison with models. From the width of the $00l$ scans, a lower limit of the average dimension along the c axis of the regularly staged regions can be inferred. This lower limit is found to be 210 Å for sample 2 and 120 Å for sample 3. It should be noted that the staging of the samples appears to be homogeneous, because diffraction (including $00l$ scans) from various spots of the samples were found to be identical.

C. X-ray equipment and cooling systems

The studies were performed using x-ray scattering from a Cu anode tube, using doubly bent focusing graphite monochromators. For sample 1, only film techniques were used, both with stationary exposures and with a precession camera. Samples 2 and 3 were initially investigated by the precession technique and also stationary exposures, and were four months later studied in more detail, also by a counter diffractometer.

The Huber diffractometer provides a vertical-axis sample rotation (ω) and detector equatorial-plane motion (σ), as well as an out-of-plane detector motion (τ). A Tracor Northern system TN-5300 is used to drive the three stepping motors and to collect the data.

The precession studies were performed with a 12-kW Rigaku rotating-anode x-ray source, and the diffractometer studies were performed with a Philips 2-kW stationary anode. For the former case, the sample cooling was achieved with cold N_2 gas from a LN_2 boiler. The temperature accuracy was rather coarse, to within several degrees. The diffractometer is equipped with a Displex DE-204H closed-cycle cryostat with a temperature reading accuracy of ±0.3 K. The absolute-temperature scale was not calibrated, but is probably correct to within 1—2 K.

For the low-temperature diffractometer runs the samples were oriented with the c axis vertical, so that the $(hk0)$ plane was confined to the horizontal plane. The longest dimension of the samples, $([110])_G$, was thus horizontal. For l scans the climbing-angle (τ) option of the diffractometer was used, moving the counter in the vertical plane. This motion was, however, restricted by the cryostat to ±25°.

At room temperature, some $00l$ and $h0l$ scans were performed, both with the sample's long dimension vertical and horizontal. Also, rocking curves to determine the mosaic spread of the samples were measured at these two settings.

The angular resolution of the diffractometer system—as determined by the monochromator mosaic and the incident- and scattered-beam collimators—can be set to Γ_{FWHM} (horizontal)$=0.3°$ and Γ_{FWHM}(vertical)$=0.55°$ (FWHM denotes full width at half maximum) at scattering angles $\sigma=35°$ and $\tau=12.5°$. A full resolution-correction procedure for the diffractometer has not yet been developed.

III. RESULTS OF OBSERVATIONS

A. The phase transition

All samples, irrespective of stage index and aging phenomena, exhibit a disordered, partly modulated liquid phase at room temperatures and down to the transition temperature T_c in the region just below 250 K. The hexagonal modulation[9] of the liquid x-ray scattering is in all cases somewhat temperature dependent. More detailed discussion of the liquid structure will appear in a planned subsequent paper.

Just below 250 K, a discontinuous transition takes place, whereby the liquid scattering disappears and Bragg scattering from ordered phases appear. The transition is clearly discontinuous, and superheating and supercooling hystereses of 3—5 K are seen when the temperature change is sufficiently slow (i.e., 1 K in 5 min). The coexistence of liquid and solid phases, previously reported,[8,9] does not occur to any appreciable extent, except during more rapid temperature changes. Examples of heating and cooling curves for sample 2 are shown in Fig. 2. Time-dependent effects, with time constants of the order of several minutes, are seen, in particular, close to T_c. The actual transition is seen to be distributed over a temperature range of about 2 K. In this region, scattering from the normal intercalant structure disappears upon heating, while liquid scattering appears (Fig. 3). Simultaneously, the scattering from graphite $(10l)_G$ and, in particular, $(11l)_G$ changes greatly (Figs. 4 and 5).

However, since the peak widths of the intercalated phase peaks do not show any variation in this region, it is believed that the finite-temperature range of the transition region reflects a spread in transition temperature due to intercalation inhomogeneities, domain-size variation, etc.

The transition temperatures for the stage-2 and -3 samples are quite similar. For sample 2 (stage 2) we found $T_{cl}=244\pm1$ K and $T_{ch}=249\pm0.5$ K, and, for sample 3 (stage 3), $T_{cl}=244.5\pm1$ K and $T_{ch}=248\pm0.5$ K. The "extra phase" (see below) appears at about 245 K upon cooling and disappears upon heating at 259 K.

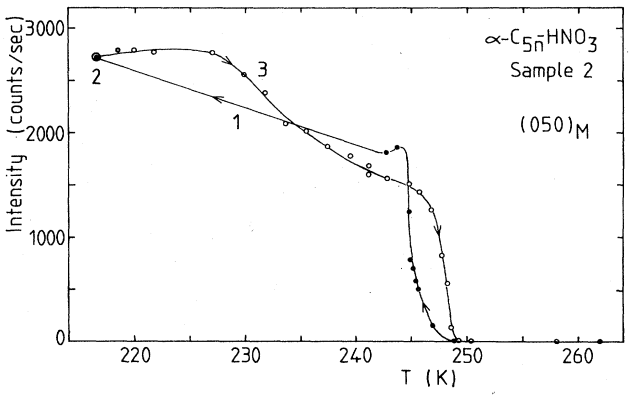

FIG. 2. Intensity of intercalant reflection $(050)_M$ vs temperature for stage 2 (sample 2) as observed in a temperature cycle of (1) cooling (●) from 262 K through T_c at a rate of 0.2 K/min, then quickly to 216.5 K (2) at 216.5 K overnight, and (3) heating (○) at a rate of about 0.2 K/min to above T_c.

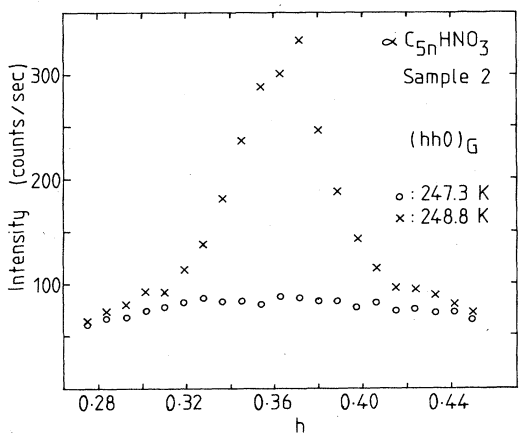

FIG. 3. Radial diffractometer scans of $(hh0)_G$ of sample 2 at 247.3 K (○) and at 248.8 K (×) during heating, showing the appearance of "liquid" scattering.

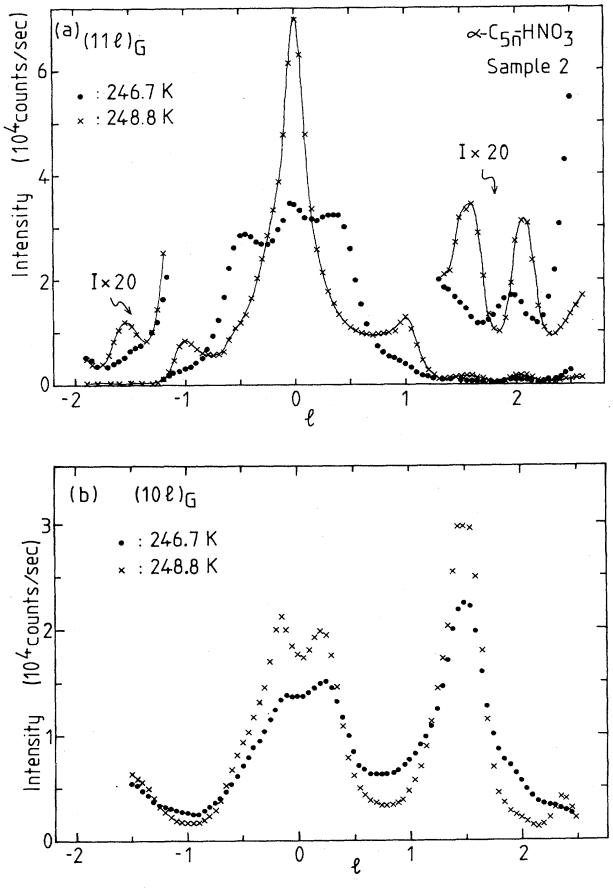

FIG. 4. Vertical diffractometer scans of graphite $(11l)_G$ and $(10l)_G$ of the stage-2 sample at 246.7 K (●) and 248.8 K (×) upon heating. l refers to a repetition distance 11.15 Å. (a) $(11l)_G$; (b) $(10l)_G$.

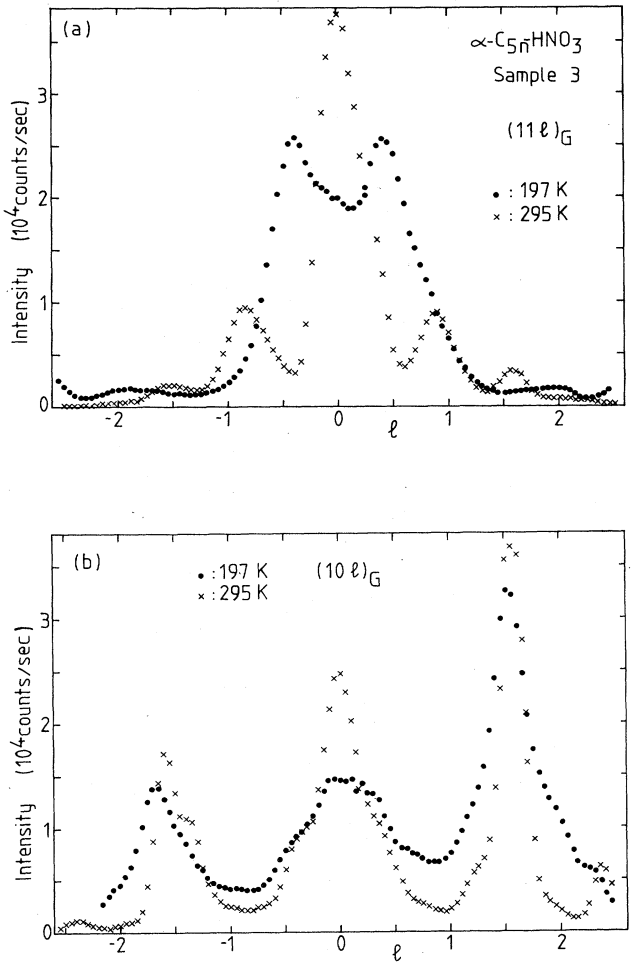

FIG. 5. Vertical diffractometer scans of graphite $(11l)_G$ and $(10l)_G$ for the stage-3 sample at 197 K (●) and 95 K (×). l refers to the same repetition distance as in Fig. 4, but the stage-3 repetition distance is 29 Å. (a) $(11l)_G$; (b) $(10l)_G$.

B. Ordered phases and aging

The actual phases observed in the ordered region below T_c turn out to be somewhat dependent on sample age, and possibly also on the detailed sample thermal history. Fortunately, however, one phase, labeled phase M in Ref. 9, which we shall refer to as the "normal phase," does appear for all samples independent of staging. It will be further described below.

The intermediate phase (I) is a phase found in the fresh stage-2 samples in a temperature region just below T_c.[9] It was indexed on a cell strongly incommensurate with the graphite lattice. However, after four months this phase had completely disappeared in sample 2, and the transition at T_c is directly from the liquid state to the normal phase M upon cooling. In sample 3, now of stage 3, traces of the intermediate phase were still seen, but it did not appear as a separable phase in a certain temperature region, but rather as a phase coexistent with the normal

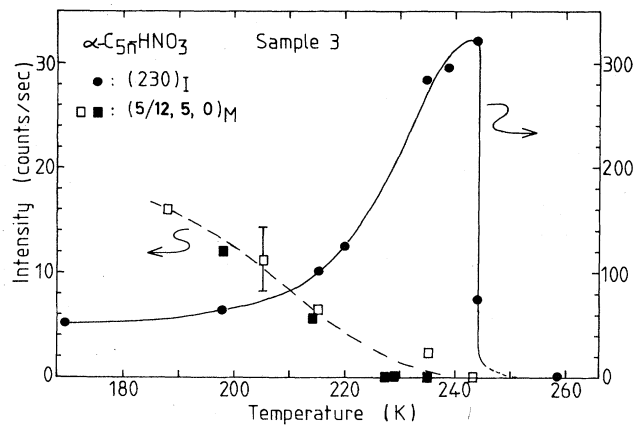

FIG. 6. For sample 3, diffractometer intensity of intermediate-phase peak $(230)_I$ (●) (scale to the right) and superlattice peak $(\frac{5}{12},5,0)_M$ (□ and ■) (scale to the left), vs temperature.

phase, as is seen from Fig. 6. The amount of the I phase depends on the thermal treatment. We conclude that the phase is primarily a property of fresh samples. No further attempts will be made in the present work to analyze it.

The normal phase (M) is a phase present in all samples at all times in some temperature range. It is the phase in the low-temperature region into which the liquid phase normally transforms upon cooling through T_c. In Fig. 7(a) we reproduce $hk0$ precession photographs showing this phase for sample 1 (stage 8). A similar photograph for the fresh sample 2 was shown in Ref. 9. Figure 7(b) depicts the indexing of the picture in 7(a) taking into account the six equivalent domains. The planar reciprocal unit cell is oblique, with the following dimensions at 213.5 K,

$$\begin{aligned}\mathbf{A}^* &= (0.698\pm0.003)\mathbf{a}_G^* - (0.1542\pm0.0009)\mathbf{b}_G^* ,\\ \mathbf{B}^* &= (0.1108\pm0.0004)\mathbf{b}_G^* ,\end{aligned} \tag{2}$$

corresponding to an oblique direct lattice with

$$\begin{aligned}\mathbf{A} &= (1.433\pm0.006)\mathbf{a}_G ,\\ \mathbf{B} &= (1.994\pm0.016)\mathbf{a}_G + (9.025\pm0.03)\mathbf{b}_G ,\end{aligned} \tag{3}$$

and five other equivalent domains. The appropriate relations are given in Appendix B. These values are close to those determined in Ref. 9 for the fresh stage-2 samples, showing that the normal-phase geometry is indeed the same.

On stationary photographs covering a larger angular region than in Fig. 7, also additional Bragg spots were seen, among them $(200)_M$ and $(0k0)_M$, with $k=10$—15. Very careful diffractometer runs were not performed to redetermine A^* and B^* of the five-month-old, low-stage samples.

The intercalated layers turn out to be correlated among themselves in the ordered phase of the low-stage samples, as discussed in Sec. IV B. The C-axis periodicity coincides with that of the graphite-lattice stacking (for the stage-2 sample), or it may even be twice of it (for the stage-3 sample).

As seen from Eqs. (2) and (3), the M phase is commensurate with the graphite lattice along **B** but not along A.

Satellite reflections would appear if the intercalant lattice interacts strongly with the graphite substrate, due to lattice modulation. This is discussed in the following section. For our structure, the incommensurability can also be monitored by careful determination of angles. For this purpose, the $(\bar{1}50)_M$ reflections of pairs of domains may be used, since they fall within 1°—2° separation on the $\langle 100\rangle_G$ axes;[9] see Appendix B. This splitting (φ) turns out to be temperature dependent, indicating a temperature-dependent incommensurability. It is shown in Fig. 8 for the stage-2 and -3 samples, as measured by the diffractometer study. The splitting saturates below about 200 K at a value around 0.7°. By contrast, the precession photographs for the stage-8 sample gave values ranging from 1.5°±0.3° at 194 K to 1°±0.3° at 243 K, and somewhat lower values for the stage-2 samples.

1. *Lock-in transition of normal phase*

In the fresh stage-2 samples, strong indication of a lock-in transition to a large supercell along **A** ($\mathbf{A}=17\mathbf{a}_G$) was found between 210 and 230 K, through the appearance of superlattice lines.[9] It turns out that this lock-in transition is also age dependent. For sample 2 in the diffractometer study, we no longer found any superlattice lines. In fact the "splitting" value of 0.7° is 35% too low to account for the fully commensurate $\mathbf{A}=17\mathbf{a}_G$, and the structure thus remains incommensurate at all temperatures.

The situation is slightly different for sample 3. There weak superlattice lines do appear at low temperatures, also four months later. An example is shown in Fig. 9. They gradually lose their intensity upon heating, and disappear between 230 and 240 K (see Fig. 6). On the other hand, also for sample 3, the low-temperature structure is not fully commensurate, because the "splitting" is lower than the theoretical value, $\varphi_c=0.915°$, of the fully commensurate case.[9]

It is easily shown that a splitting angle φ of 0.7° requires that $A=16.96a_G$ rather than $17a_G$, and also that precession data for sample 1, with $\varphi>\varphi_c$, are consistent with an A value $>17a_G$. In neither case is the structure entirely commensurate. The implications of this are discussed later.

2. *Additional phase by aging*

A further complication of this system is the occurrence of an extra phase, increasing in importance upon aging. In Fig. 7(a) several fairly strong spots may be identified which are not indexable on either of the structures already described. In fact, these spots were not found on pictures of the fresh stage-8 sample,[8] but are quite pronounced after one year of storage. On the fresh stage-2 samples, spots belonging to this phase were seen also, although

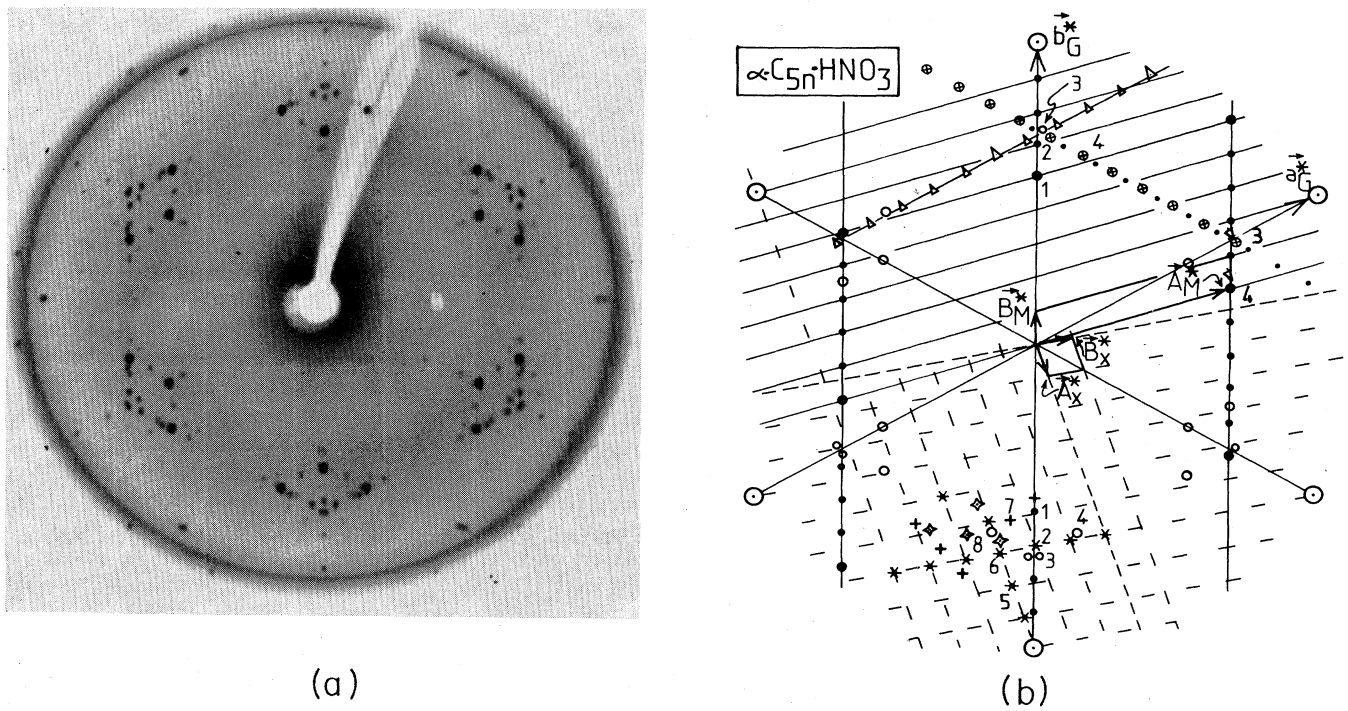

FIG. 7. (a) Precession photograph of $(hk0)$ of sample 1 at 223 K. (b) This figure is an attempt to clarify the indexing of the spots of (a): *The upper half* of the figure contains spots related to the M phase only, one domain being illustrated by the reciprocal net and the larger solid circles (●). Contributions from equivalent domains are shown by various symbols (●, ⊗, △, ▽, ●). In order to identify the six characteristic groups of stronger spots (○ ○ ○ ○ ○ ○) of (a), spots designated ○ are added throughout. The graphite spots are indicated by ⊙. *The lower half* contains some of the additional spots due to the X phase, one domain being illustrated by the dashed reciprocal net and the asterisks (*). Contributions from equivalent domains are shown by ✦ and +, primarily in the lower-left quadrant. Identification of some numbered spots is as follows: (1) $(050)_M$, (2) $(060)_M$ and $(620)_X$, (3) $(\bar{1}50)_M$ doublet, (4) $(100)_M$, (5) $(730)_X$, (6) $(630)_X$, (7) $(430)_X$, and (8) $(600)_X$.

weak, but after four months they are quite strong both for sample 2 and sample 3. Examples of such peaks are seen in Fig. 7(a) and also in Fig. 10.

The extra peaks can be indexed on a commensurate lattice with the reciprocal-lattice dimensions

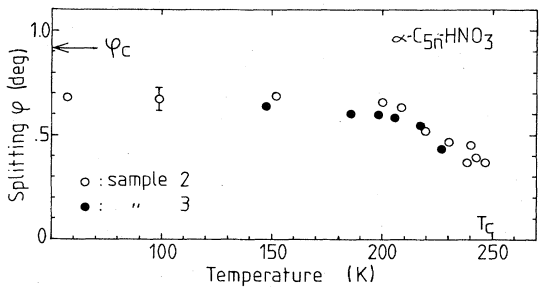

FIG. 8. Angular splitting (φ) by diffractometer scans of $(\bar{1}50)_M$ of pairs of domains [spot (3) of Fig. 7(b)] vs temperature for sample 2 (○) and sample 3 (●). Commensurate value $\varphi_c = 0.915°$ is indicated. The FWHM of each peak of the doublet is 0.42° for sample 2 and 0.50° for sample 3.

$$\mathbf{A}_X^* = \tfrac{1}{24}(2\mathbf{a}_G^* + \mathbf{b}^*), \quad \mathbf{B}_X^* = \tfrac{1}{24}(-2\mathbf{a}_G^* + 3\mathbf{b}^*), \tag{4}$$

and their equivalents corresponding to a direct lattice,

$$\mathbf{A}_X = 9\mathbf{a}_G + 6\mathbf{b}_G, \quad \mathbf{B}_X = -3\mathbf{a}_G + 6\mathbf{b}_G, \tag{5}$$

with two equivalent other domains, as given in Appendix B.

It is characteristic that this phase does not vanish at the same temperature as the "normal" lattice. For both samples 2 and 3, it has a higher transition temperature upon heating ($T_{ch} = 259$ K). The extra peaks are, however, influenced considerably by the transition of the normal structure, as is seen from Fig. 10. Also the extra structure may be supercooled.

We consider it likely that the upper of the two calorimetric anomaly peaks observed[4] in α-C_{5n}-HNO_3 is due to the extra phase. It is quite probable that the extra phase is due to some chemical species evolved by slow reaction within the intercalated graphite. According to Fuzellier,[5] HNO_3 is easily dissociated into $NO_2 + H_2O$, and also higher oxides such as N_2O_5 or N_2O_4 may be present. The presence of NO_2 is readily seen from the brownish color of the gas surrounding the specimen in the capillaries. As this phase is commensurate with the

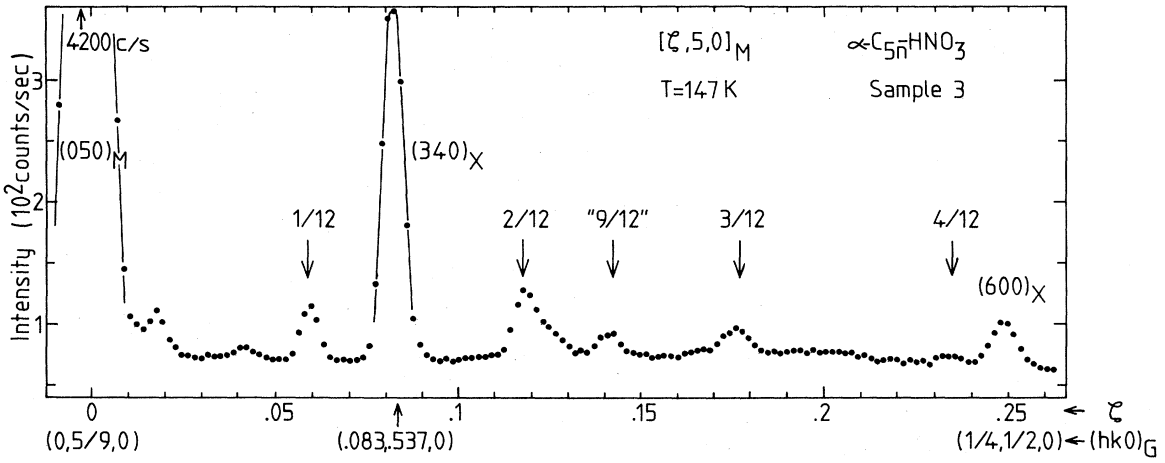

FIG. 9. Sample-3 diffractometer scan along $[\zeta 50]_M$ at 147 K showing one normal-phase peak, $(050)_M$, two extra phase peaks, $(340)_X$ and $(600)_X$, and some superstructure peaks, $(n/12)$. Referred to the graphite lattice, the scan is along $[\zeta, \frac{1}{9}(5-2\zeta),0]_G$.

graphite and not with the normal phase M, it must exist intercalated at locations by itself, rather than mixed into the normal phase. The dip in Fig. 10 at T_{ch}, however, shows that its ordering is influenced either by the normal-phase ordering or by the graphite-layer sliding (Sec. IV A).

IV. INTERLAYER EFFECTS

A. Graphite-layer stacking and sliding

The graphite-layer stacking is normally denoted by the letters A, B, and C such that if the origin of layer A, say, is taken at the (hexagonal) position $X_H=0, Y_H=0$, B layers are shifted by $X_H^B=\frac{1}{3}, Y_H^B=\frac{2}{3}$, and C layers by $X_H^C=\frac{2}{3}, Y_H^C=\frac{1}{3}$.

Nixon *et al.*[6] concluded from their x-ray study that the stage-2 α-C_{5n}-HNO_3 could be described by the c-axis sequence

$$A/AB/BC/C \tag{6}$$

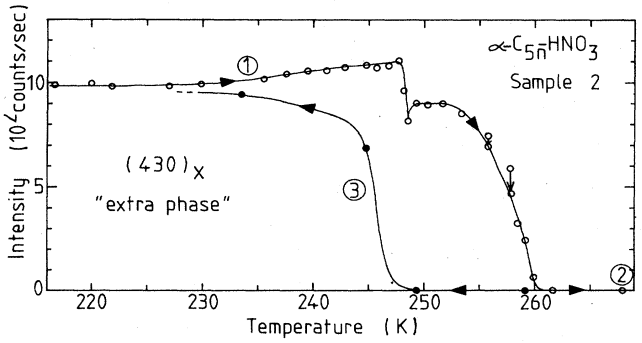

FIG. 10. Sample-2 diffractometer intensity of extra phase peak, $(430)_X$ [spot (7) of Fig. 7(b)] vs temperature for one temperature cycle; (1) heating at 0.2 K/min, (2) 1 h above 268 K and (3) cooling at 1 K/min.

(where / indicates an intercalant layer), with a distance I_c between nearest intercalant layers being 11.15 Å, corresponding to a repetition length of 33.45 Å. However, Fuzellier[5] found that the sequence for stage 2 is instead

$$A/AB/B\ , \tag{7}$$

with a repetition length of 22.30 Å.

The l dependence of the $(10l)_G$ scattering of our stage-2 sample above T_c is, in fact, in agreement with (7), although we cannot entirely exclude the presence of some small percentage of (6). Such a stacking is, furthermore, in agreement with the l dependence of the intercalant scattering.

For stage 3, Nixon *et al.* found a stacking

$$A/ABA/ACA/A\ , \tag{8}$$

with $I_c=14.48$ Å and a repetition distance of 28.96 Å. The $(10l)_G$ scattering from our stage-3 sample is in agreement with this, although the intercalant scattering may point to a doubling of this repetition unit (see below). These are the stacking sequences above 250 K.

However, as already noted by Parry,[7] the intercalant ordering at T_c is accompanied by a major change of the scattering from $(11l)_G$; some changes are, in fact, also seen for $(10l)_G$. The variation across the transition region is seen from Figs. 4 and 5, showing l scans of $(10l)_G$ and $(11l)_G$. The convention is taken to refer to a c axis of 11.15 Å in both cases. For 110 the contribution is approximately halved upon passing T_c for both samples. Simultaneously, the $l=1$ peak practically disappears, and strong shoulders develop at $l=\frac{1}{2}$ for the stage-2 sample. Similarly, for the stage-3 sample the contributions at $l\simeq 0.85$ and 1.60 disappear, and peaks appear for $l\simeq 0.40$. For $00l$ scattering, however, such a change was not observed. We notice that the intercalant contribution to $(11l)_G$ should be negligible because of the incommensurability.[14] Since typical intercalant intensities are less than one-tenth of the graphite-lattice intensities, the intercalant contribution to $(10l)_G$ is also quite small. The effect de-

TABLE II. Sliding-model intensities. Ratio $R(hkl)=(I_{\text{unslided}}-I_{\text{slided}})/(I_{\text{unslided}}+I_{\text{slided}})$ for stage-2 sample calculated for the graphite sliding model, compared with observations using $I_{\text{unslided}}=I_{\text{high temp}}$ and $I_{\text{slided}}=I_{\text{low temp}}$ (see Fig. 4). The sliding parameters $x=0.2$ and $y=0.05$ used for the calculations give a good fit for the $l=0$ cases and a fair semiquantitative fit elsewhere. The case designated by an asterisk (*) is contaminated by stage-3 contribution (cf. Fig. 5).

	$l\rightarrow$	0	$\frac{1}{2}$	1	$\frac{3}{2}$	2	$\frac{5}{2}$
$R_{\text{obs}}(11l)$		0.34	−0.4	0.5	0.4*	0.4	−0.6
	$x+y$						
$R_{\text{calc}}(11l)$	0.2	0.20	−1.0	0.20	−1.0	0.20	−1.0
	0.25	0.33	1.0	0.33	−1.0	0.33	−1.0
	0.30	0.49	−1.0	0.49	−1.0	0.49	−1.0
$R_{\text{obs}}(10l)$ or $R_{\text{obs}}(01l)$		0.12	−0.13	−0.23	0.14	−0.5	∼0.0
	x,y						
$[R_{\text{calc}}(10l)+R_{\text{calc}}(01l)]/2$	0.15, 0.10	0.08	−0.022	−0.26	0.08	−0.69	0.05
	0.20, 0.05	0.14	−0.027	−0.30	0.10	−0.73	0.07
	0.25, 0	0.17	−0.032	−0.33	0.12	−0.76	0.09

picted in Figs. 4 and 5 is therefore due to the graphite lattice. Since, for graphite stacking involving only the pure A, B, and C layers, $(11l)_G$ should obey the same extinction rules as $(00l)_G$, one is led to conclude, as did Parry,[7] that some graphite layers are driven out of the pure hexagonal stacking below T_c.

In fact, the observed curves may be semiquantitatively reproduced by applying a model where the A/A (B/B) sandwich transforms into A/A' (B/B') with A' shifted of the order of $0.2\mathbf{a}_G+0.05\mathbf{b}_G$ (or the equivalent) relative to A. Comparison between intensity-ratio calculations and observations for the stage-2 case is given in Table II. For stage 2, the sequence assumed below T_c is

$$A/A'B'/B'', \tag{9}$$

so that the relation between A' and B' is the same as between A and B. (For the stage-3 case, it is, similarly, $A/A'B'A'/A''C''A''$.) To retain the repetition length of 22.30 Å, it is also necessary that the shifts alternate plus and minus from layer pairs to layer pairs, thus involving an "antitranslational" ordering scheme of graphite layers, making $B''\equiv B$. We notice that neighboring A and B layers may be considered bound units which interact with neighboring units via the intercalant layers. Their ordering scheme below T_c is "antitranslational" (see Fig. 11). It would be natural to try and describe the system by use of a one-dimensional model involving interaction between neighboring units. The same applies for the stage-3 case, with the units being ABA and ACA layer groups.

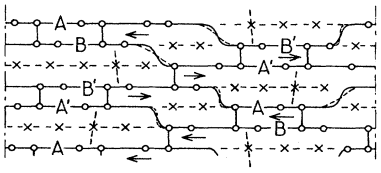

FIG. 11. Stacking schemes, domain boundaries, and graphite-layer sliding at T_c for a stage-2 intercalation compound. Carbon-atom sites are rendered schematically by open circles; vertical bars between A and B layers are shown to indicate stiffness. Nearly vertical dashed bars indicate possible HNO_3 molecular-plane orientation connected with graphite sliding. Horizontal and vertical scales are out of proportion.

The graphite-layer sliding represents a most unusual effect, not reported for other graphite intercalation compounds. Because of the strength of the in-layer graphite bonding the sliding motion most likely involves dimensions of the order of the domain sizes, probably several hundreds of angstroms. Within the Daumas-Hérold domain model the motion may be pinned at the domain boundaries, as illustrated in Fig. 11. In addition, there will be transverse elastic resistance to the sliding at the sidewalls of the domains.

B. Intercalant interlayer correlation

In the *disordered* or liquid state there is no correlation between intercalant layers, even for the stage-2 case. This can be seen from the precession pictures containing the c^* axis. The liquid streaks parallel to the c^* axis are diminishing only slowly for increasing l, and there is no periodic modulation.

In the *ordered* region the *normal-structure* peaks show a modulation along l somewhat dependent upon the thermal history. Only a limited number of the peaks were studied.

Examples of l scans of intercalant scattering for the stage 2 sample are shown in Figs. 12 and 13. As is seen, the $(0kl)_M$ digrams indicate a considerable amount of in-

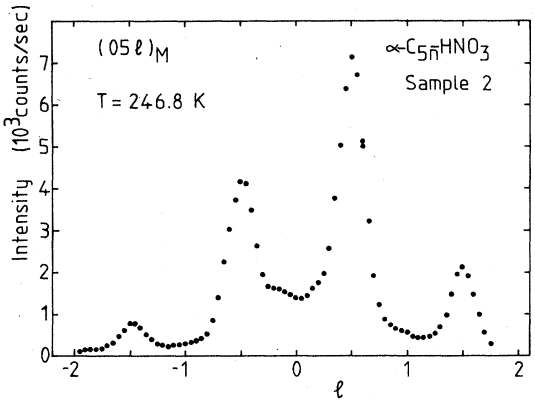

FIG. 12. Vertical diffractometer scan for sample 2 of intercalant $(05l)_M$ at 246.8 K upon heating.

terlayer correlation. It is noteworthy that $(05l)_M$ shows a minimum intensity at $l=0$ and maxima at $l=\pm 0.5$, whereas $(06l)_M$ has the opposite characteristics (not shown).

The modulation may be interpreted by allowing for a pronounced in-plane shift X_M, Y_M of the intercalant lattice from layer to layer. The detailed determination of X_M, Y_M can only be performed with full knowledge of the actual intercalant molecular ordering. For instance, an in-layer structure factor will enter. However, from the ratio

$$I(0\,k\,0)_M / I(0\,k\,\tfrac{1}{2})_M$$

for $k=5$ and 6, assuming nearest-layer correlations to be dominant, one can derive an order of magnitude for Y_M, giving $Y_M \simeq 0.14$.

The scattering from $(10l)_M$ is more thermal-treatment dependent. In Fig. 13 we show three scans, with one thermal cycle through T_c between the one at 99.5 K and the one at 246.7 K. Thus the X_M is less well defined than

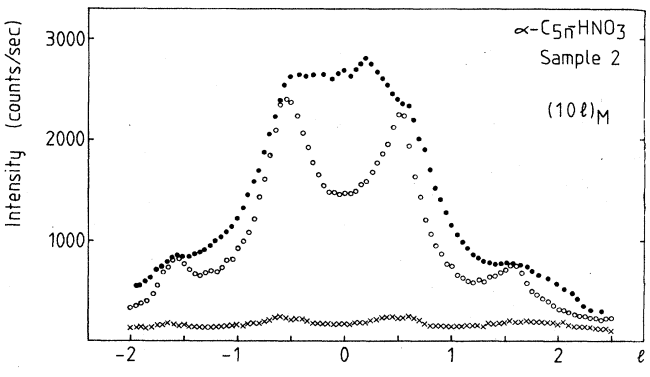

FIG. 13. Vertical diffractometer scans for sample 2 of intercalant $(10l)_M$ at two different stages of thermal history. One run at 99.5 K (●) is followed by one temperature cycle to above T_c, cooling again to 216.6 K, and then at 246.7 K (○) and 248.8 K (×) on heating.

Y_M, a fact which is probably connected with the incommensurability along $\mathbf{A}_M$. An analysis of the 246.7-K observation along similar lines as for Y_M gives values of X_M in the range $\pm(0.25$—$0.30)$.

It is probably significant that the values of X_M, Y_M thus derived are in fair qualitative agreement with a shift of $(\frac{2}{3},\frac{4}{3})_G$ referred to the graphite lattice. (See Appendix B for coordinate transformation.) This shift corresponds to a translation along [120] from an A-layer site to the nearest equivalent B-layer site.

The stage-3 sample was less extensively studied for the intercalant stacking. Qualitatively, $(10l)_M$ scans showed very little modulation, whereas $(05l)_M$ did show well-defined maxima at $l=0.2$, 1.0, and 1.4, and minima at $l=0$, 0.35, 0.8, and 1.2. The latter periodicity indicates a intercalant repetition period of $4\times I_c \simeq 58$ Å.

The scattering from the *extra phase* (of sample 2) always showed a monotonic l dependence from maxima at $l=0$, with a FWHM normally $(1.0$—$1.2)l$ units. This shows that the species of the extra phase are weakly correlated, with a correlation length not more than to the first-neighboring layers, and that there is no in-plane shift from layer to layer.

V. DISCUSSION AND CONCLUSIONS

The normal, aging-independent behavior of the α phase of nitric acid intercalated in graphite is that the liquid phase transforms by a first-order transition into an ordered phase which is commensurate with the graphite lattice is one direction (**B**) and incommensurate in the other (**A**). The transition temperatures are staging independent, being $T_{cl}=244\pm 1$ K upon cooling, and $T_{ch}=249\pm 1$ K upon heating. For the stage-2 sample, the most extensively studied case, the stacking sequence is $A/A'B'/B$ with a repetition distance $C=2I_c=22.30$ Å. Intercalant layers are correlated along **C**, with a shift from layer to layer which is somewhat thermal-treatment dependent along **A**, but less so along **B**.

The observed l-scan diffraction is consistent with a rational intercalant stacking shift of $\frac{2}{3}(\mathbf{a}_G+2\mathbf{b}_G)$, corresponding to the line AB_2 of Fig. 14, so that the intercalant configuration at point A of layer 0, say, is identical to the configuration at point B_2 of layers ± 1 (perhaps except for a minor tilting angle.)

At lower temperature the tendency for intercalant modulation by the graphite lattice to create a superstructure with $\mathbf{A}=17\mathbf{a}_G$ lessens with time, and full commensurability is not achieved.

The intercalant ordering at T_c is accompanied by an unexpected sliding motion of graphite layers, so that the layers on either side of an intercalant layer are shifted relative to each other. This shift between A and A' in an A/A' sandwich could be determined semiquantitatively to be of the order of $(0.2,0.05)_G$ or $(0.05,0.2)_G$, amounting to a shift of 0.45 Å. Such shifts are indicated in Fig. 14. It is noteworthy that they are essentially parallel to or normal to **B**.

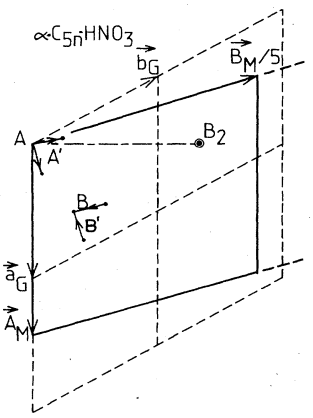

FIG. 14. Four cells of a graphite layer with origin at A, together with a $\frac{1}{5}$ unit cell of the intercalant normal phase M, showing $\mathbf{A}_M$ and $\frac{1}{5}\mathbf{B}_M$. Relative shift of intercalant layers for stage 2 is of the order of $A-B_2=\frac{2}{3}(\mathbf{a}_G+2\mathbf{b}_G)$. Possible graphite-layer slidings A-A' (B'-B) are indicated.

The mechanism for the sliding interaction is somehow mediated by the intercalant ordering. We notice that the HNO_3 molecules are believed to have an orientation essentially normal to the graphite layers.[11,12] Furthermore, we notice that cooling through T_c shortens the c axis by 0.04—0.05 Å.[15] A molecular tilt upon cooling through T_c of about 5.8° around a horizontal axis (with a molecular outer dimension 7.80 Å−3.35 Å=4.45 Å) can account for the c-axis reduction.

In fact, such a tilt, with the HNO_3 molecules acting as a ball bearing between graphite layers, does account for a shift of 0.45 Å. Such a model requires that bonding exists between the HNO_3 molecules and the graphite layers. To preserve the c-axis periodicity the tilting angle must alternate in sign along the c axis. The tilting model may be checked only by careful studies of $00l$ scattering through T_c.

We have not yet determined the molecular ordering of the low-temperature phase. This will be the subject of a subsequent paper. The intercalant layer of the M phase contains five molecules,[9] altogether with $5\times2+5\times3=25$ positional and orientational parameters to be determined, assuming rigid molecules. The interlayer correlation strongly influences the actual interpretation of the $hk0$ data set, and several hkl reflections may be required for a full structural determination. An added complication is that the interlayer correlation depends on the thermal history.

The one-direction incommensurability observed may possibly point to a molecular chain structure. Chaining of HNO_3 molecules by hydrogen bonds is, of course, quite likely and probably occurs in solid HNO_3.[16]

The observed incommensurability may be accounted for by assuming commensurate regions along **A** separated by walls or domain boundaries[17] ("stripe domains"). For instance, the presence of both modulation peaks (sample 3) and a splitting angle $\varphi<\varphi_c$ is consistent with a structure involving regions with unit cells with $\mathbf{A}=17\mathbf{a}_G$ separated by walls with $\mathbf{A}=16\mathbf{a}_G$. One $16\mathbf{a}_G$ unit in average per twenty-four $17\mathbf{a}_G$ units just corresponds to an observed $\mathbf{A}=(17\times24+16)/25\,\mathbf{a}_G=16.96\mathbf{a}_G$.

Since the **B** axis is commensurate, the molecular chains, if present, would have to run along **B**, with some zig-zagging in order to accomodate the five molecules (4.7 Å linear extension each[11]) within the 20.1-Å B-axis length. The graphite-layer sliding would best be normal to the chains.

ACKNOWLEDGMENTS

One of us (E.J.S.) would like to acknowledge partial financial support from Norges Teknisk-Naturvitskaplege Forskingsråd. Technical assistance by Mr. L. Deschamps, J. P. Wagner, and Madame H. Albouze is gratefully acknowledged.

APPENDIX A: NOTATION AND RELEVANT DATA

We use the following notation: index G, graphite lattice; index I, intermediate phase; index M, normal phase; index X, extra phase. Graphite lattice $a_G=2.46$ Å. The intercalant-layer distance along the c axis, often called the "repeat distance," $I_c=11.15$ Å, is used as a reference length. All l indices refer to this length. Observed repeat distances from $(00l)$ at room temperature are 11.16 ± 0.02 Å for state 2, and 14.51 ± 0.04 Å for stage 3. Stage mixing is determined in terms of relative volumes from the intensity ratios of the pairs

$$(003)_{\text{stage 2}}\text{-}(00\,3.06)_{\text{stage 3}}\,,$$

$$(004)_{\text{stage 2}}\text{-}(00\,3.75)_{\text{stage 3}}\,,$$

and

$$(006)_{\text{stage 2}}\text{-}(00\,6.13)_{\text{stage 3}}\,,$$

assuming vertical HNO_3 molecules in a concentration corresponding to C_{5n}-HNO_3. This gave $(11\pm3)\%$ stage 3 in sample 2 and $(4.5\pm2)\%$ stage 2 in sample 3.

APPENDIX B: INDEX AND POSITION TRANSFORMATIONS

Normal-phase intercalant reflections $(hk0)_M$ referred to the reciprocal unit cell given by

$$\mathbf{A}_M^*=p\mathbf{a}_G^*+q\mathbf{b}_G^*\,,$$

$$\mathbf{B}_M^*=r\mathbf{b}_G^*\,,$$

with $p\simeq12/17$, $q\simeq-24/(9\times17)$, and $r=1/9$, and their five graphite symmetry equivalents may be transformed into a graphite reference frame $\mathbf{a}_G^*,\mathbf{b}_G^*$ according to the following table:

Domain	Symmetry operation	$(hk0)_G$
1	Identity E	$hp, hq+kr, 0$
2	C_3	$-(hq+kr), h(p+q)+kr, 0$
3	C_3^2	$-h(p+q)-kr, hp, 0$
4	σ_b	$-hp, h(p+q)+kr, 0$
5	$\sigma_{a\text{-}b}$	$-(hq+kr), -hp, 0$
6	σ_a	$h(p+q)+kr, -(hq+kr), 0$

The intercalant direct-lattice unit cell is described by

$$\mathbf{A}_M = t\mathbf{a}_G ,$$

$$\mathbf{B}_M = u\mathbf{a}_G + v\mathbf{b}_G ,$$

with $t=1/p\simeq 17/12$, $u=-q/p$, $1/r\simeq 2$, and $v=1/r=9$.

Transformations between position coordinates $(X_M, Y_M, 0)_M$ and $(X_G, Y_G, 0)_G$ are given by

$$X_G = X_M t + Y_M u ,$$

$$Y_G = Y_M v ,$$

and

$$X_M = \frac{1}{t}X_G - \frac{u}{v}\frac{1}{t}Y_G ,$$

$$Y_M = \frac{1}{v}Y_G .$$

The extra phase reciprocal- and direct-lattice unit cells will occur as three equivalent domains:

Domain	Operation	
1	E	$\mathbf{A}_X^* = \frac{1}{24}(\mathbf{a}_G^* - 3\mathbf{b}_G^*)$ $\mathbf{B}_X^* = \frac{1}{24}(3\mathbf{a}_G^* - \mathbf{b}_G^*)$ $\mathbf{A}_X = -3(\mathbf{a}_G + 3\mathbf{b}_G)$ $\mathbf{B}_X = 3(3\mathbf{a}_G + \mathbf{b}_G)$
2	C_3	$\mathbf{A}_X^* = \frac{1}{24}(3\mathbf{a}_G^* - 2\mathbf{b}_G^*)$ $\mathbf{B}_X = \frac{1}{24}(\mathbf{a}_G^* + 2\mathbf{b}_G^*)$ $\mathbf{A}_X = 3(2\mathbf{a}_G - \mathbf{b}_G)$ $\mathbf{B}_X = 3(2\mathbf{a}_G + 3\mathbf{b}_G)$
3	C_3^2	$\mathbf{A}_X^* = \frac{1}{24}(2\mathbf{a}_G^* + \mathbf{b}_G^*)$ $\mathbf{B}_X^* = \frac{1}{24}(-2\mathbf{a}_G^* + 3\mathbf{b}_G^*)$ $\mathbf{A}_X = 3(3\mathbf{a}_G + 2\mathbf{b}_G)$ $\mathbf{B}_X = 3(-\mathbf{a}_G + 2\mathbf{b}_G)$

The angle φ between the type-$(\bar{1}50)_M$ reflections of domains 1 and 5, say, may be obtained from the cross product of the two vectors

$$\mathbf{R}_1 = -p\mathbf{a}^* + (-q+5r)\mathbf{b}^* ,$$

$$\mathbf{R}_5 = (-q+5r)\mathbf{a}^* - p\mathbf{a}^* ,$$

giving

$$\sin\varphi = \frac{\sqrt{3}(p^2 - q^2 - 25r^2 + 10qr)}{2(p^2 + q^2 + 25r^2 - 10qr + pq - 5pr)} .$$

*Permanent address: Avdeling for Fysikk og Matematikk, Norges Tekniske Høgskole, Universitetet i Trondheim, N-7034 Trondheim—NTH, Norway.

[1]H. Fuzellier, J. Melin, and A. Hérold, Mater. Sci. Eng. **31**, 91 (1977).
[2]A. R. Ubbelohde, Proc. R. Soc. London, Ser. A **304**, 25 (1968); **327**, 289 (1972).
[3]F. L. Vogel, Carbon **14**, 175 (1976).
[4]A. Dworkin and A. R. Ubbelohde, Carbon **16**, 291 (1978).
[5]H. Fuzellier, Ph.D. thesis, Université de Nancy, 1974.
[6]D. E. Nixon, G. S. Parry, and A. R. Ubbelohde, Proc. R. Soc. London, Ser. A **291**, 324 (1966).
[7]G. S. Parry, Mater. Sci. Eng. **31**, 99 (1977).
[8]R. Moret, R. Comès, G. Furdin, H. Fuzellier, and F. Rousseaux, Mater. Res. Soc. Symp. Proc. **20**, 27 (1983).
[9]E. J. Samuelsen, R. Moret, R. Comès, H. Fuzellier, M. Klatt, M. Lelaurain, and A. Hérold, Synth. Met. **10**, 13 (1984).
[10]W. Rüdorff, Z. Phys. Chem. B **45** 42 (1939).
[11]P. Touzain, Synth. Met. **1**, 3 (1979/80).
[12]H. Pinto, M. Melamud, O. Shahal, R. Moreh, and H. Shaked, Physica (Utrecht) **121B**, 121 (1983).
[13]M. S. Dresselhaus and G. Dresselhaus, Adv. Phys. **30**, 175 (1981).
[14]One may, for instance, consult the transformation table of Appendix B to confirm that $(110)_G$ will not coincide with any spot from the M phase.
[15]M. Bottomley, G. S. Parry, and A. R. Ubbelohde, Proc. R. Soc. London, Ser. A **279**, 291 (1964).
[16]V. Luzzati, Acta Crystallogr. **4**, 120 (1951).
[17]V. L. Pokrovsky and A. L. Talapov, Zh. Eksp. Teor. Fiz. **78**, 269 (1980) [Sov. Phys.—JETP **51**, 134 (1980)].

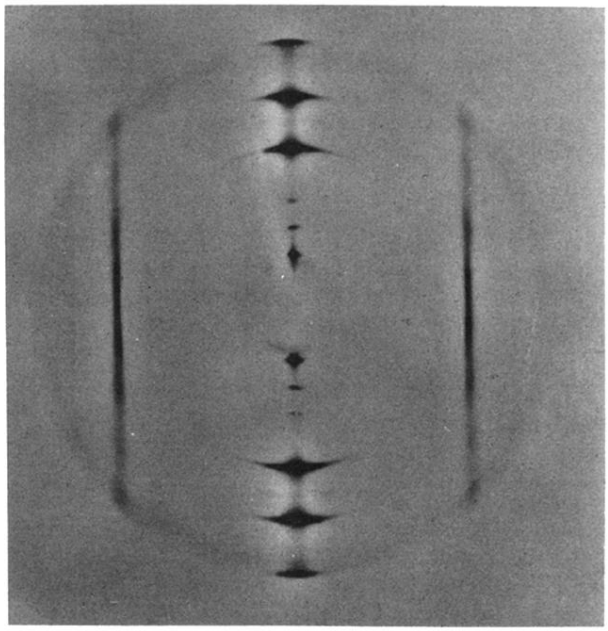

FIG. 1. Precession photograph of fresh sample 2 at 225 K showing a section containing the graphite $(00l)_G$ up to $l=5$, and the intercalant $(10l)_M$, showing l modulation. C-axis mosaic spread is seen.

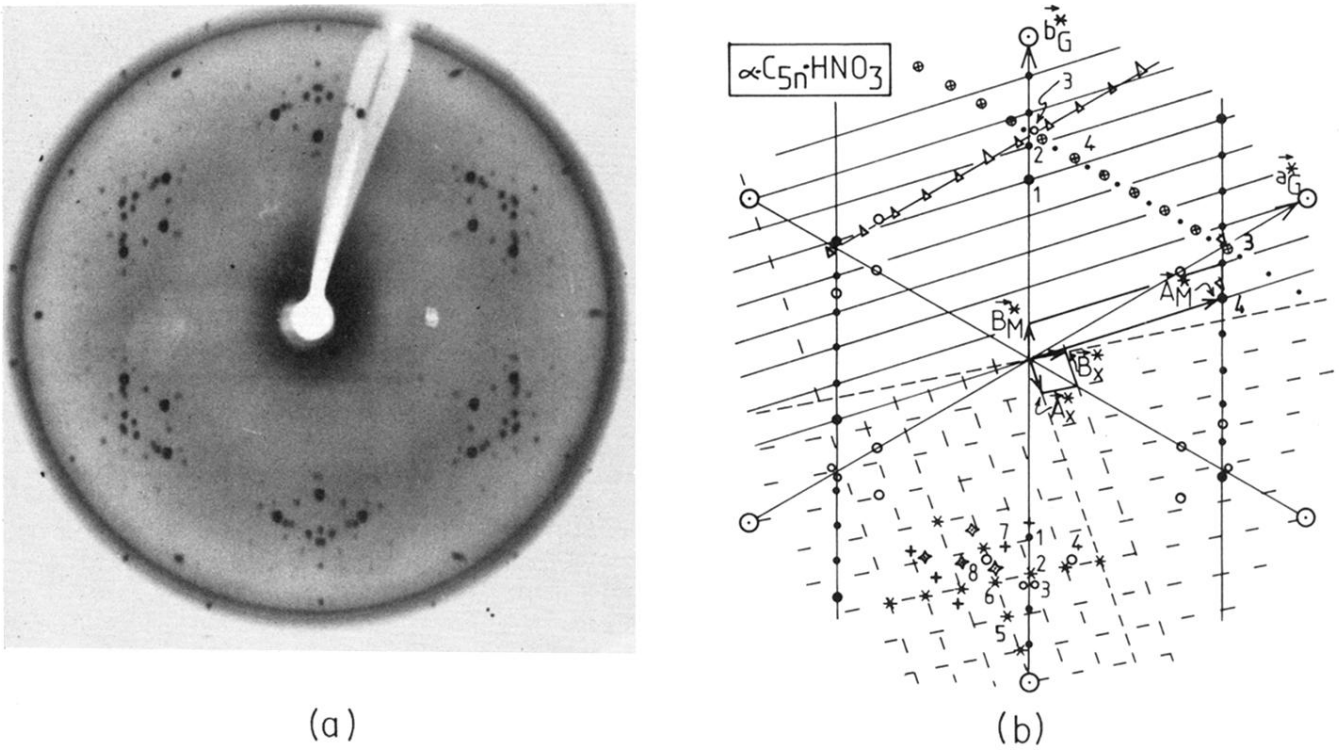

FIG. 7. (a) Precession photograph of ($hk0$) of sample 1 at 223 K. (b) This figure is an attempt to clarify the indexing of the spots of (a): *The upper half* of the figure contains spots related to the *M* phase only, one domain being illustrated by the reciprocal net and the larger solid circles (●). Contributions from equivalent domains are shown by various symbols (●, ⊗, △, ▽, ●). In order to identify the six characteristic groups of stronger spots (○ ○ ○ ○ ○ ○) of (a), spots designated ○ are added throughout. The graphite spots are indicated by ⊙. *The lower half* contains some of the additional spots due to the *X* phase, one domain being illustrated by the dashed reciprocal net and the asterisks (*). Contributions from equivalent domains are shown by ✦ and +, primarily in the lower-left quadrant. Identification of some numbered spots is as follows: (1) $(050)_M$, (2) $(060)_M$ and $(620)_X$, (3) $(\bar{1}50)_M$ doublet, (4) $(100)_M$, (5) $(730)_X$, (6) $(630)_X$, (7) $(430)_X$, and (8) $(600)_X$.